Available online at https://asric.africa/engineering-sciences
ASRIC Journal on Engineering Sciences Vol.6(1)(2025) 37-51

FEM Analysis of the Effect of Geometrical Radius on the Force Capacity of Unreinforced Masonry walls under Out-Of-Plane Monotonic Loading

John Mary Joseph Yiga[1], Moses Matovu[1], Allan Ray Okodi[1],

[1]Department of Civil and Environmental Engineering, Makerere University,
yigajmj@gmail.com, mmatovujr@gmail.com, allan.okodi@mak.ac.ug

Corresponding Author: yigajmj@gmail.com,

Received 18 July 2025; revised 14 August 2025; accepted 23 October 2025

Abstract

The susceptibility of unreinforced masonry (URM) walls to out-of-plane (OOP) failure under lateral forces from earthquakes and high winds continues to be a critical concern in ensuring structural resilience and occupant safety. While curved wall construction has gained increasing global adoption for its architectural, functional, and spatial advantages, current design provisions are predominantly formulated for straight and orthogonal geometries, leaving the flexural performance of curved URM walls analytically underrepresented. This study conducts a numerical investigation into the geometrical curvature effect on the force capacity of URM walls using a three-dimensional brick-to-brick finite element approach in ABAQUS/CAE, implemented through the Simplified Micro-Modelling technique. The methodology involved a three-step process: first, a monotonic quasi-static simulation of a full-scale straight wall was performed to calibrate and validate the model; second, the validated model was extended to curved walls with varying projection radii; and third, the resulting force–displacement responses were analyzed to assess structural performance. The results show that curvature substantially improves OOP response, with yield pressure increasing from 3.0 kPa for the straight wall to 7.4kPa for the 1000mm projection wall (approximately 150% gain), while yield displacement reduced from 9mm to 2.2mm (approximately 75% reduction), indicating enhanced stiffness. Furthermore, curved walls exhibited superior ductility, energy absorption, and stable post-yield behavior due to geometric stiffening and the development of in-plane compressive membrane stresses, which delayed crack propagation and improved load-bearing capacity. These findings provide a validated predictive framework for understanding the structural performance of curved URM walls, highlighting curvature as an effective means of enhancing structural efficiency, resilience, and toughness in masonry design, with direct implications for developing performance-based seismic codes, guiding innovative architectural forms, and optimizing the use of locally available materials in sustainable construction.

Keywords: Curved Masonry walls, Finite Element Modelling, Out-Of-Plane loads

1. Introduction

Masonry construction remains prevalent worldwide, accounting for approximately 70% of the total building inventory (Wang et al., 2018). This is largely attributed its affordability, durability, ease of construction, cultural significance, and ability to provide thermal comfort in diverse climates (Huang et al., 2024).

Masonry structures are exposed to both out-of-plane and in-plane loading during the occurrence of natural hazards like earthquakes and storms (Noor-E-Khuda et al., 2016). Although much effort has been directed towards the in-plane shear behaviour of masonry walls as the primary mechanism of the lateral load transfer (Zeng et al., 2023), the vulnerability of masonry structures to failure under OOP

load is still one of the critical issues; a case in point, during the 2010/2011 Canterbury earthquakes, (Walsh et al., 2017) reported that the failure of URM cavity walls in two-way bending accounted for 57% of all OOP wall failures. This vulnerability poses serious structural, health, and safety risks. However, research into improving OOP performance has been limited, leaving critical gaps in understanding and mitigating these risks.

Without relying on reinforcement, modifying wall geometry presents an underexplored opportunity to augment lateral resistance through thoughtful architectural design. While most research on improving the OOP capacity of masonry has focused on reinforcement strategies (Fam et al., 2015; Galati et al., 2005; Parajuli & Ghimire, 2021) and enhancements in material properties (Maccarini et al., 2018; Iqbal J., 2021), the structural influence of curvature has received comparatively little analytical attention. But there is a strong suggestion of its potential in traditional constructions. The curved wall geometry has been used long before the present in buildings like the Hakka houses in China (Briseghella et al., 2019), Bhunga houses in India (Samali et al., 2011), Yomata houses in Malawi, and rammed earth houses in Argentina (Jinwuth et al., 2011). These enduring forms suggest that curvature may contribute to stability under lateral loading; an idea echoed in recent numerical studies (Caddemi et al., 2017); (Altunişik et al., 2018), but still lacking in systematic investigation.

Current design considerations, and codes such as the (Eurocode 6 - Part 3, 2006) and (BS5628-Part1, 1992), predominately assume straightness in masonry walls; neglecting the complexities introduced by walls with curved geometries. Consequently, this assumption cannot be seamlessly extended to curved walls; as they would yield inaccurate predictions due to the oversimplification and conservatism evident in design codes (Tariq et al., 2023). This therefore warrants the re-evaluation and modification of these design codes to account for a broader design scope with emerging architectural innovations that challenge traditional paradigms. This study builds on earlier contributions while addressing unresolved gaps that shape its objectives and methods. Research on straight masonry walls is extensive, but studies on curved walls remain limited, with most insights extrapolated from straight-wall behaviour.: (Samali et al., 2011) examined unreinforced adobe walls with square and circular geometries using static tilt tests. The circular wall showed 11% higher resistance, hinting at performance benefits from curvature. However, curvature was not isolated, as aspect ratio effects were not controlled. To address this, (Jinwuth et al., 2011) used pushover tests on circular walls, producing capacity curves that captured deformation and failure loads. While confirming earlier trends, their study also lacked direct straight-to-curved comparisons; furthermore, the investigation into the variations of geometrical curvature was not done. Insights from straight-wall investigations, by (Vaculik & Griffith, 2017) who tested C-shaped URM brick walls under airbag loading, establishing pressure-displacement relationships, propose a displacement-based seismic design method for two-way spanning walls. A methodology that is transferable to the numerical investigation of how geometrical curvature affects the force capacity of URM walls.

Taking insights from related structures, (Avasthi & Rai, 2021, 2022) implemented micro modelling in ABAQUS to simulate and dynamically characterize one-fourth scale masonry arches. Their finite element results closely matched experimental mode shapes and natural frequencies, though parametric variations in geometrical curvature were not explored, highlighting a research gap. (Abdulla et al., 2017) successfully replicated (Vaculik & Griffith, 2017) C-shaped URM wall experiments using Simplified Micro-Modelling (SMM) in ABAQUS, accurately capturing out-of-plane flexural response and enabling parametric studies on two-way spanning walls with potential extension to curvilinear configurations. by (Noor-E-Khuda et al., 2016) investigated pre-compression, apertures, aspect ratio, and support conditions using ABAQUS explicit FEM. While effective for out-of-plane behaviour, their reliance on macro modelling limited resolution of local interactions and interface mechanics, constraining detailed insight into failure initiation and propagation. It is worth noting that most literature discussed here focused on straight walls and related structures like arches, it is the intention of this study that the insights drawn are extended to curved walls.

Curvature is derived from the moment-curvature relationship, which describes a structural element's response to bending moments, influenced by material properties and cross-sectional geometry (MacGregor, 2018); in this context, curvature is linked to material strengths (Timoshenko, 1993). In this research study, curvature is defined in terms of the geometrical radius, quantifying the deviation of

a wall from a straight-line form before the application of any loads (Adiels, 2016). Unlike traditional definitions that associate curvature with bending behavior under applied forces, this study treats curvature as an inherent geometric property of the wall. This distinction allows for a clearer examination of how initial geometry influences structural performance, independent of load-induced deformations. For a uniform curvature($\boldsymbol{\kappa}$) is defined as $\boldsymbol{\kappa = 1/R}$; the determination of $\boldsymbol{R}$, relies on easily measurable features of the curve, including the curve length, s, the wall projection, $\boldsymbol{h}$ and the $\boldsymbol{c}$, which is the shortest distance between two points of a known curve length. When the curve length; s, is held constant while varying the radius; $\boldsymbol{R}$ of the wall, the concept of wall projection becomes critical in defining the geometric properties of the curve (Association, 2005)-

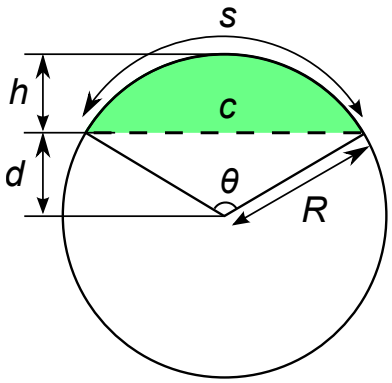

Fig. 11: Geometrical features of a circle.

The relationship between projection with radius of curvature is mathematically expressed in ***Equation 1***. A larger radius results in a gentler curve with lower curvature, while a smaller radius leads to a sharper, more pronounced curve with higher curvature. Building on this, the fundamental assumption in this study is that a straight wall can be considered a unique curved wall with an infinitely large radius; ($\boldsymbol{R} = \infty$), meaning its curvature is zero. Since curvature measures how much a shape deviates from being straight, a straight line represents the case of no deviation/projection; ($\boldsymbol{h} = 0$). This makes it the least curved shape possible, contrasting with circles or other curves that have a finite radius.

Based on this assumption therefore, we are able to explore a range of curved walls; which is the purpose of the research study. This is the reason why the numerical validation of models is founded using the experimental studies of a straight wall as will be found out later in this paper. The relationship between projection with radius of curvature is best expressed in the formular (Haukaas, 2006) - derived from the graph in ***Figure 2*** The second term, $\boldsymbol{c^2/8h}$, dominates when the span c is large compared to the projection h, indicating that the radius increases significantly as the curve becomes flatter.

$$R = \frac{h}{2} + \frac{c^2}{8h} \qquad (1)$$

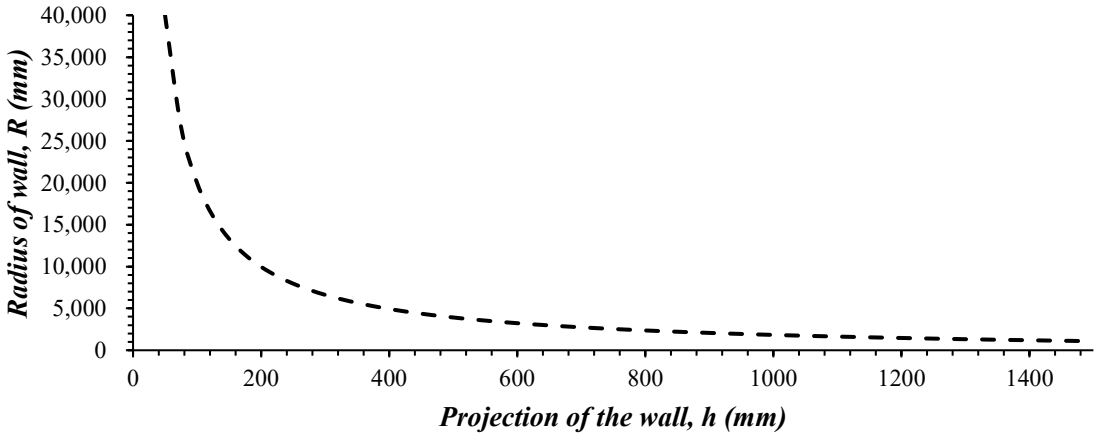

Fig. 2: *Projection vs Radius of curvature*

2. Methodology

This paper examines the impact of out-of-plane force capacity of Unreinforced Masonry (URM) walls. Simplified Micro-Modelling A three-dimensional brick to brick modelling was applied through the finite element ABAQUS/ CAE program. The research procedure was done in three steps:

i. To simulate and validate a numerical model, a quasi-static monotonic test was initially simulated on a straight wall;
ii. After successful validation, the model was furthered to provide a series of parametric analysis on a curved URM wall; and
iii. Later, force-displacement responses of the developed models have been measured to determine how the curvature affects the structural performance.

2.1. Modelling theory

Masonry is a composite anisotropic product because the material composing it has different mechanical properties, which in effect makes it difficult to predict its behavior (Bolhassani et al., 2015). Nevertheless, as the role of computational mechanics and materials has become important in the development of structural engineering, studies have driven into the field of micromechanical behavior and the optimization of constitutive models in various loading scenarios (Alam et al., 2009); making numerical models as plausible substitutes to physical experiments as highlighted by (Baluch et al., 2012). Finite Element Modeling (FEM) is the most popular of the numerical modelling methods used in the walls. Here, there are three methods of simulation of masonry i.e. Macro, Simplified Micro and Micro modeling (Lourenco et al., 2006) -see ***Figure 3*** the choice of which depends on the required accuracy and detail (Jiang et al., 2010).

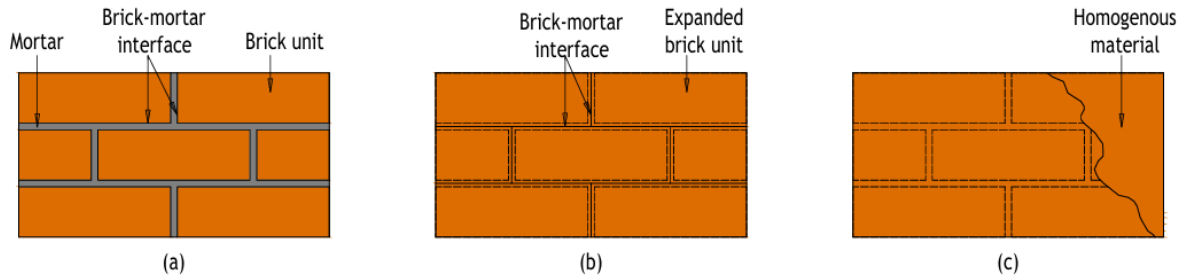

Fig. 3*: Finite element modelling approaches: (a) detailed Micro-model; (b) simplified Micro-model; (c) Macro-model*

The units and mortar are represented as continuum elements in the Micro-model approach and discontinuum elements as unit-mortar interfaces (Avasthi and Rai, 2021). In the application of the Macro-model approach, the masonry is treated as a homogeneous material where units and mortar are not differentiated, the material properties are taken as the average property of masonry constituents and the masonry is represented as a continuum of elements. (Abdulla et al., 2017). The most promising of these is the Simplified Micro-modelling which only tries to model masonry at the level of structural components; since the cracks and frictional slips are supposed to occur in the joints of mortar. Mortar joints in this are zero-thickness interface elements, and the bricks are expanded, and represented as solid elements (Chang et al., 2021). In such a way, it is possible to balance computational efficiency and the accurate representation of wall crack patterns in an optimal way.

The anisotropies are characteristics of masonry materials, whose values depend almost entirely on the direction of the mortar joints; i.e. bed and head joints, which potentially are planes of structural weakness. According to (Asteris et al., 2014), joint orientation, joint dimensions, and joint properties may determine the mode of failure, either local at the joints or both at the joints and the units, which is, in fact, a part of the complex behaviour of masonry structures. This means that the quality of the simulated structural behaviour of masonry is extremely sensitive to the quality of material properties (Teschemacher et al., 2023b). As far as the simulation of 3D masonry is implemented within the frame of the Simplified Micro Modelling approach, one should resort to plasticity-based constitutive models

(which are stressed by (Abdulla et al., 2017). The following discussion gives failure modes of the models.

2.1.1. Surface-based Cohesive Behavior Model

The model explains the linear and fracture behaviour of bed and head mortar joints; taking into consideration the traction-separation properties between masonry units (Noor-E-Khuda et al., 2016) see ***Figure 4***. Therefore, the model of constitutive relies on the plasticity of the dilatant interface that has the ability to model the initiation and propagation of interface fracture under normal and shear stresses combined (Jiang et al., 2010).

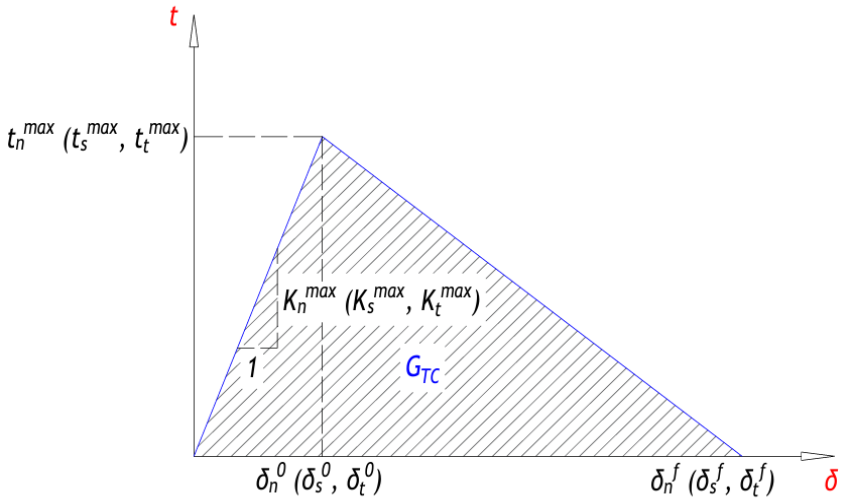

Fig. 4: *Traction separation response of masonry joint interfaces (Abdulla et al., 2017)*

2.1.1.1. Elastic Response of the Joint Interfaces

Prior to any damage, the joint interfaces' initial behaviour depends on a linear traction-separation relationship. An elastic stiffness matrix equation **t=Kδ**, which relates the directional tractions of the surface and their associated separations (see Eq. (2)), is used to numerically depict this behaviour (Abdulla et al., 2017).

$$\boldsymbol{t} = \begin{Bmatrix} t_n \\ t_s \\ t_t \end{Bmatrix} = \begin{bmatrix} K_{nn} & 0 & 0 \\ 0 & K_{ss} & 0 \\ 0 & 0 & K_{tt} \end{bmatrix} \begin{Bmatrix} \delta_n \\ \delta_s \\ \delta_t \end{Bmatrix} = \boldsymbol{K\delta} \qquad (2)$$

The components of the stiffness matrix, **K**, include the stiffnesses of brick and mortar under identical boundary conditions. Eqs. (3) and (4) define the equivalent stiffness coefficients for these joint surfaces as functions of the elastic moduli of the mortar and the masonry unit as well as the mortar joint thickness (Lourenço et al., 2006).

$$K_{nn} = \frac{E_u E_m}{h_m (E_u - E_m)} \qquad (3)$$

$$K_{ss} = K_{tt} = \frac{G_u G_m}{h_m (G_u - G_m)} \qquad (4)$$

$$G = \frac{E}{2(1+v)} \qquad (5)$$

Mortar is modelled as an isotropic material using Eq. 5, where $\boldsymbol{G_u}$ and $\boldsymbol{G_m}$ are the brick-unit shear modulus and mortar joint shear modulus, respectively (MPa), $\boldsymbol{h_m}$ is mortar thickness (mm), $\boldsymbol{E_u}$ and $\boldsymbol{E_m}$ are the elastic moduli of masonry brick units and mortar, respectively (MPa), and **v** is the Poisson's ratio.

2.1.1.2. Plastic Response of the Joint Interfaces

The initiation of damage is established using the quadratic stress criterion, which is satisfied when the quadratic stress ratios of the masonry interfaces reach a value of one (Campilho et al., 2008) (see Eq. (6)). With this, crack propagation ensues.

$$\left(\frac{t_n}{t_n{}^{max}}\right)^2 + \left(\frac{t_s}{t_s{}^{max}}\right)^2 + \left(\frac{t_t}{t_t{}^{max}}\right)^2 = 1 \qquad (6)$$

t_n^{max} is the maximum permissible traction stress in the perpendicular direction (tensile strength of masonry joints), t_s^{max} is the maximum permissible traction stress along the primary shear plane (shear strength of masonry joints), and t_t^{max} is the maximum permissible traction stress along the secondary shear plane (shear strength of masonry joints), all expressed in MPa. Because it takes mixed-mode loadings into account, this criterion is appropriate for forecasting the beginning of deterioration in masonry joint interfaces. According to the Benzeggagh-Kenane (BK) law (Benzeggagh M, 1996), the critical mixed-mode fracture energy dissipation at failure G_{TC} (N/mm) is acceptable when the critical fracture energies of both shear directions (mode II and mode III), which are typical of masonry joints, are the same. According to the Mohr-Coulomb criteria, the critical shear stress τ_{crit} at which a joint failure occurs is represented in Eq. (7) for assessing the tensile strength of brick wall connections to determine their propensity to break under strain.

$$\tau_{crit} = c + \mu\sigma_n \qquad (7)$$

Where c represents the cohesion at brick joints (MPa), μ is the frictional coefficient between brick joints, and σ_n is the normal contact pressure stress at the brick joint interfaces (MPa).

2.1.2. Elastic Behavior of Expanded Units

The elastic modulus of the enlarged masonry units must be adjusted in order to guarantee an equal elastic response between them and the original masonry assemblage (i.e., containing both units and mortar) (Jiang et al., 2010). This modification depends on the geometric properties of the masonry assemblage as well as the moduli of elasticity of the original mortar and masonry units. For this aim, a number of scholars have put out formulae that assume a homogeneous stress distribution inside the masonry elements and a stack bond between masonry units (Khattak et al., 2021). This study used Eq 8 by Jiang et al. (2010) to simplify the variables.

$$E_{adj} = \frac{HE_uE_m}{nh_u E_m + (n-1)h_m E_u} \qquad (8)$$

Where E_{adj} is adjusted elastic modulus (MPa), n is the number of courses in the brick wall, h_u is the height of the masonry brick unit (mm) and H is the height of the brick wall (mm).

2.1.3. Drucker-Prager plasticity model

This is used to model masonry units' nonlinear response to compressive force. This model allows for the prediction of possible compressive failures in masonry buildings by accounting for both isotropic hardening and softening behavior. The Mohr-Coulomb criteria were initially extended by the Drucker-Prager (DP) model, which was mainly designed to estimate failure stress in frictional materials like rocks and soils (D. C. Drucker, 1952). Later on, it was improved to include the compressive yield criteria, specifically addressing the impact of hydrostatic compaction pressure. Both linear and non-linear deformations are taken into consideration by the parametrically described DP plasticity model (Simulia, 2014). The evolution of the yield surface during non-linear deformations is based on the uniaxial compression yield stress characteristic of the masonry assemblage (Teschemacher et al., 2023a), whereas important parameters such as flow stress ratio, dilation angle, and friction angle must be precisely specified within the linear criterion (Zeng et al., 2021).

2.2 Material Model

In order to account for the linear and non-linear behavior displayed by enlarged units and their interfaces, a complex 3D finite element simplified micro-model was used in ABAQUS-CAE. The experimental study by Vaculik and Griffith (2017), which tested a C-shaped brick wall (***Figure 5***) under

out-of-plane force circumstances, provided insights for the validation of the straight FE Models. The return walls, that create the flanges, were 0.45 meters long and 2.5 meters high, while the main web portion of the wall was 4 meters long and 2.5 meters high. The brick unit dimensions were 230 x 110 x 76 mm, the wall thickness being 110 mm, and the mortar joints are set at 10mm with a mix ratio of 1:2:9 (cement: lime: sand); all of these measurements are in line with the experimental investigation. The bond pattern conformed to a half-overlap stretcher bond. ***Tables 1*** and ***2*** provide the values utilized for the material characteristics.

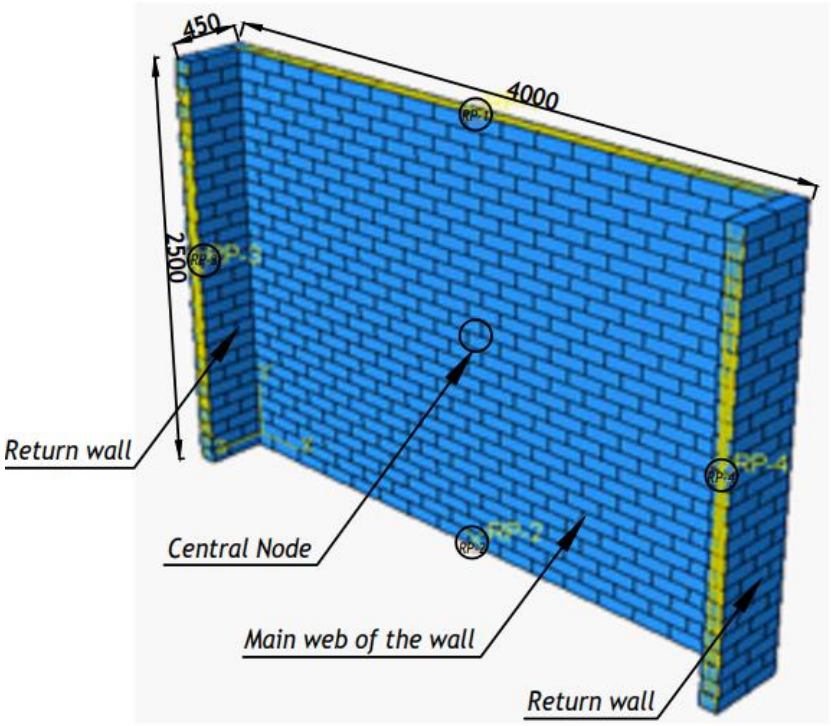

Fig. 53: *Assembly of the Simplified Micro Model for the Straight wall adopted for the study*

2.2.1. Material Properties

(a) The expanded masonry units

Table 1: *Material properties for the masonry units*

Category	Parameter	Value	Data Source
Elastic behavior of masonry units	Density	1,900kgm^3	Estimated
	E_b	52,700MPa	(Vaculik & Griffith, 2017)
	E_j	420MPa	
	Poisson's ratio	0.15	(Khattak et al., 2021)
Onset Plastic behavior (Drucker Prager model)	Friction angle	36°	(D. C. Drucker, 1952)
	Flow stress ratio	1.0	Assumed
	Dilation angle	10°	(Misir & Yucel, 2023)
Hardening behavior of masonry units	Stress-strain compression curve	see *Error! Reference source not found.*	(Kaushik et al., 2007)
	Fracture energy	0.08N/mm	(Abdulla et al., 2017)

Category	Parameter	Value	Data Source
Damage assessment (Quads damage criterion)			For mode-dependent stress components using the **BK** law (Benzeggagh M, 1996)
	Tensile strength	1.18MPa	(Vaculik & Griffith, 2017)
	Shear strength	1.65MPa	Assumed to be **1.4** of the tensile strength (Lourenço et al., 2006)

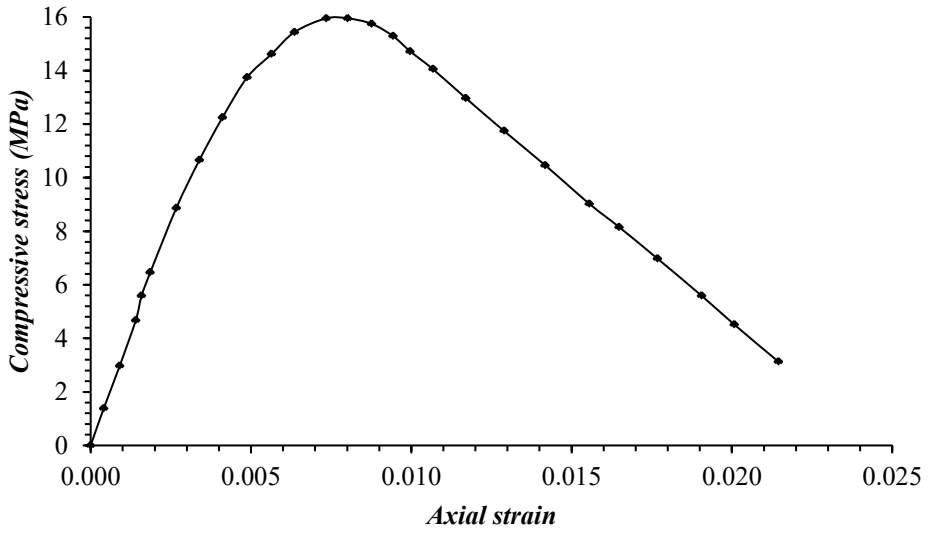

Fig. 6: *Stress-strain compression curve for the masonry wall (Kaushik et al., 2007)*

(b) The joint interfaces

A surface-based coherent approach was employed. In this a node-to-surface discretization technique that uses finite sliding formulation was used to characterize the contact interactions between neighboring masonry units (Wani et al., 2023). In the adopted setup, two distinct contact property assignments were created to correspond to the major surfaces of the expanded masonry unit; i.e. Top, and Bottom. The interaction characteristics listed in ***Table 2*** were used in these assignments.

Table 2: *Interaction properties for the joint interfaces*

Failure behavior	Parameter	Value	Data Source
Tangential behavior	Friction coefficient	0.75	Estimated
	Shear stress limit (i.e. cohesion)	0.04MPa	(Maria et al., 2018)
Normal behavior	Contact pressure-overclosure relationship	-	Hard contact behavior (Bolhassani et al., 2015)
Cohesive behavior (Stiffness coefficients)	K_{nn}	42N/mm^3	Calculated from Equations (2) and (3) in ***Section 2.1.1.1*** of this report (Lourenço et al., 2006).
	K_{ss}	17N/mm^3	
	K_{tt}	17N/mm^3	
Damage assessment (quadratic stress criterion)	Fracture energy	0.012N/mm	(Vaculik & Griffith, 2017)
	Maximum normal stress (tension)	0.12MPa	(Lourenço et al., 2006).
	Maximum nominal stress (shear)	0.17MPa	(Lourenço et al., 2006).
	Viscosity coefficient	0.002	(Abdulla et al., 2017).

The tangential behaviour of the mortar joints was defined by the penalty friction formulation, taking into account the dimensionality of isotropy. In order to prevent penetration and the transmission of

tensile stress between the mortar joints, the normal behaviour, utilized the hard contact behaviour, defined by the contact pressure-overclosure relationship (Bolhassani et al., 2015).

2.2.2. Boundary Conditions and Loading Scheme

On the outside face of the web wall section, lateral loads were applied monotonically (quasi-statically) as a pressure distribution, with a total magnitude of 0.05kN/m² during a step time length of one second. The top and bottom margins of the wall, as well as the ends of the return walls, were modeled as simply supported (Richter & Brehm, 2009). Control reference points are established to define the boundary conditions and are kinematically coupled to the wall surfaces, with all six degrees of freedom constrained.

2.2.3. Validation of Straight Wall

3D hexahedral shaped eight node linear (type C3D8R) brick elements with decreased integration and hour glass control (Simulia, 2014) were used to simulate the extended units (Mathew et al., 2021). To iteratively achieve equilibrium in each increment, the ABAQUS/Standard solver used a generic non-linear static technique directed by the Newton-Raphson algorithm (Simulia, 2014). The applied pressure was calculated by dividing the total forces in the reaction frame by the wall's web's surface area after the analyses (Abdulla, 2019). The wall's reactions were shown graphically as a relationship between the OOP displacement and the applied pressure. The appropriate mesh size was chosen based on a mesh sensitivity study, with the 5×2×2 mesh identified as one with the highest convergence with laboratory results by (Vaculik & Griffith, 2017). see Figure 7

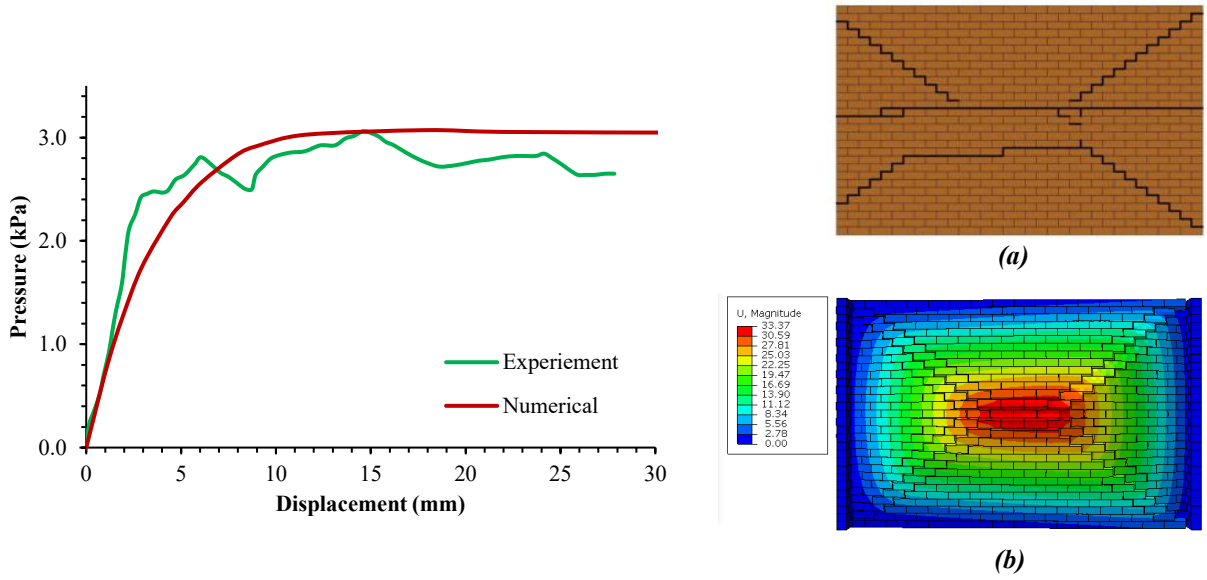

***Fig. 74**: Relationship between displacement of the web section of the wall and the applied pressure*

While force-displacement curves capture global structural response, they disregard localized behavior such as crack initiation, hinge formation, and non-uniform displacement fields (Godio & Beyer, 2019). Such features are of the utmost significance in masonry, in which failure has often been induced by local instabilities (Young & Budynas, 2002). From the results of the numerical models, observed patterns confirmed that both capacity and failure mechanisms were accurately reproduced by the model.

Failure in the test (Vaculik & Griffith, 2017) was characterized by mid-height horizontal cracking along the web wall, together with stepped diagonal cracks propagating towards the corners (***Figure** 7*). The numerical model simulated this crack pattern extremely well (***Figure 7b***), validating its ability to accurately model the initiation, and propagation of cracks. However, unlike in the experiment in which there were distinct diagonal cracks, the numerical analysis exhibited a field of distributed diagonal cracks. This is attributable to uncertainties in material properties; some of which were estimated from

literature due to a lack of experimental data. Another factor is the model's assumption of uniform unit-mortar interface properties (Abdulla et al., 2017) and the neglect of the likely variability in joint strength because of workmanship, material quality, and local stress concentrations (Plevris & Asteris, 2014). Overall, the numerical model has adequate fidelity, and it is suitable for use in parametric analyses.

3. Parametric analysis

Four different wall projections were selected for this analysis, utilizing a validated model, as the basis: 250mm, 500mm, 750mm, and 1000mm as shown in ***Fig***. For each projection, the wall's run length was fixed at 4m, and the height was maintained at 2.5m, ensuring consistent dimensions across the geometries.

The radii of the curved walls corresponding to each projection were calculated using a predefined relationship between wall radius and projection, as illustrated in ***Fig. 1****1*. This allowed for a systematic analysis of how increasing curvature impacts the structural response of the walls. Importantly, aside from the geometrical variations, all other model parameters, such as material properties, return walls, bonding patterns, and boundary conditions, were kept constant and aligned with the settings described in ***Section 2.1***. This ensured that any observed differences in performance could be attributed solely to the changes in geometry. The focus in this study is on typical weak mortar/strong brick masonry systems (Basha & Kaushik, 2015), which are commonly used to represent clay brick masonry in practice.

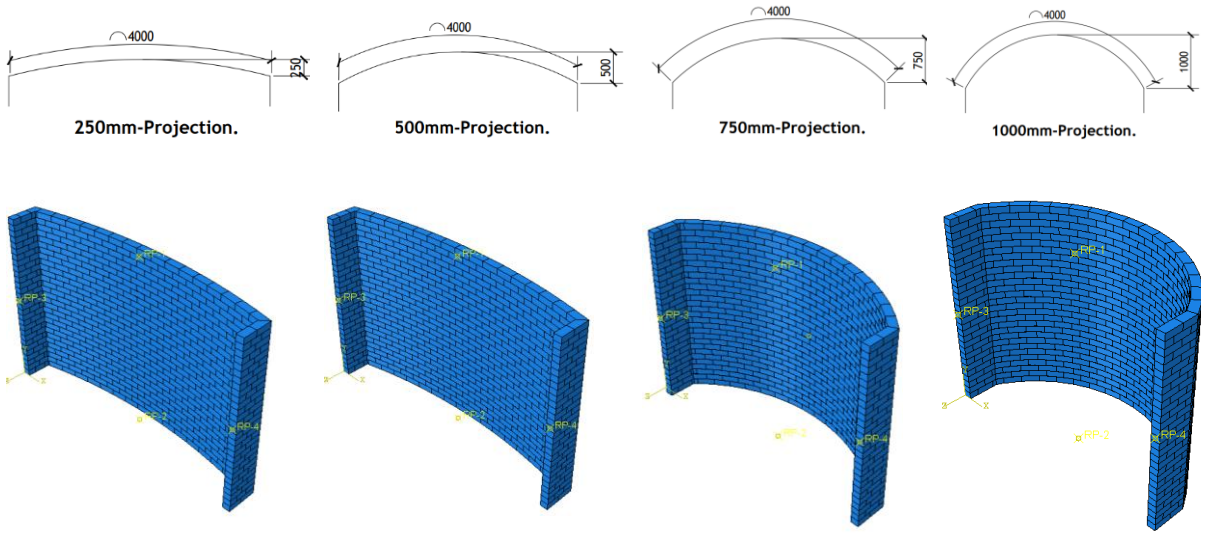

Fig. 8: *Selected models of masonry walls with different geometrical curvatures in ABAQUS*

4. Results and Discussion

The pressure-displacement responses presented in ***Fig*** reveal a consistent trend in which yield pressure increases with wall curvature. Yield pressure, defined as the point of departure from initial linear stiffness, provides a rational measure of effective resistance prior to the onset of cracking and nonlinear deformation. Across all specimens, pressure initially rises steeply with displacement, corresponding to the elastic response zone, followed by a plateau as the wall material undergoes inelastic deformations.

The numerical straight wall exhibits a yield pressure of approximately 3.0kPa, attained at a displacement of 9mm. This relatively low value highlights the structural inefficiency of flat URM walls under out-of-plane loading, where resistance is governed largely by tensile rupture of mortar joints and interface slip. With the introduction of curvature, however, yield capacity increases markedly. The 250mm-projection wall achieves a yield pressure of 4.8kPa (a 60% increase relative to the straight wall). The 500mm-projection wall develops 5.2kPa, representing an 8% gain over the 250mm wall. Similarly, the 750mm-projection wall reaches 6.2kPa, a further 19% improvement, while the 1000mm-projection wall exhibits the highest capacity at 7.4kPa, corresponding to an overall 150% increase compared to the straight wall benchmark.

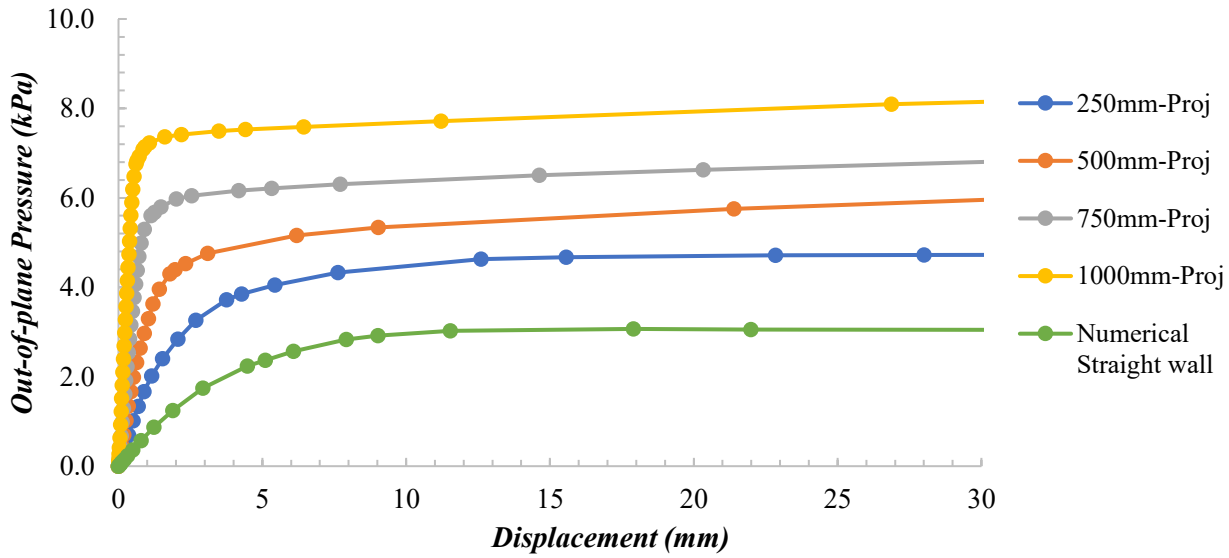

Fig 9: *Force displacement results for the masonry wall with different geometrical curvatures*

These results highlight the role of geometric stiffening and membrane effects in curved masonry walls. Increasing curvature enhances the wall's effective flexural rigidity, making its behavior closer to that of a shallow shell, also supported by (Calladine, 2007), (Urugal, 2018). In this configuration, part of the applied out-of-plane pressure is resisted not only through bending but also by the development of in-plane compressive membrane stresses (Morandi et al., 2008), which delay onset cracking and elevate the yield threshold. The curved configuration limits lateral deflections, thereby reducing the effective slenderness (span-to-thickness ratio) and increasing the structural stiffness and stability of the wall under lateral pressures.

Displacements recorded at yield reinforce this interpretation. The 250mm-projection wall yielded at 7.6mm, while larger projections exhibited progressively lower displacements: 3.1mm for the 500mm wall (a 59% reduction), 2.5mm for the 750mm wall (a 19% reduction), and 2.2mm for the 1000mm wall (a further 12% reduction). The steeper elastic slopes in the pressure-displacement curves confirm an increase in initial stiffness with projection radius also affirmed by (Chang et al., 2021) (see Fig). The increased area under the curve for higher projections indicates enhanced toughness, an essential parameter for seismic design where cyclic out-of-plane demands dominate performance (Abdulla et al., 2017).

Failure mode analysis indicates that crack patterns remain generally similar across all curvatures, manifesting as diagonal yield-line mechanisms consistent with the boundary conditions as attested to by (Osorio et al., 2024) (see Fig). However, as projection increases (500-1000mm), the regions of high displacement become progressively smaller and more localized at the wall center. This suggests that increased curvature enables more efficient redistribution of internal stresses and confines large displacement demands to a narrower region (Khaleel et al., 2021). Notably, the 1000mm-projection wall demonstrates the most uniform contour distribution, with high-deformation zones confined to the central region, reflecting its enhanced stiffness and shell-like response.

In summary, yield pressure evaluation confirms that geometrical curvature significantly enhances out-of-plane flexural capacity through mechanisms of geometric stiffening, membrane action, and improved stress redistribution, rather than classical arching. These effects collectively produce higher yield thresholds, reduced yield displacements, and greater post-yield ductility, underscoring the structural efficiency of curved geometries for unreinforced masonry under lateral loading.

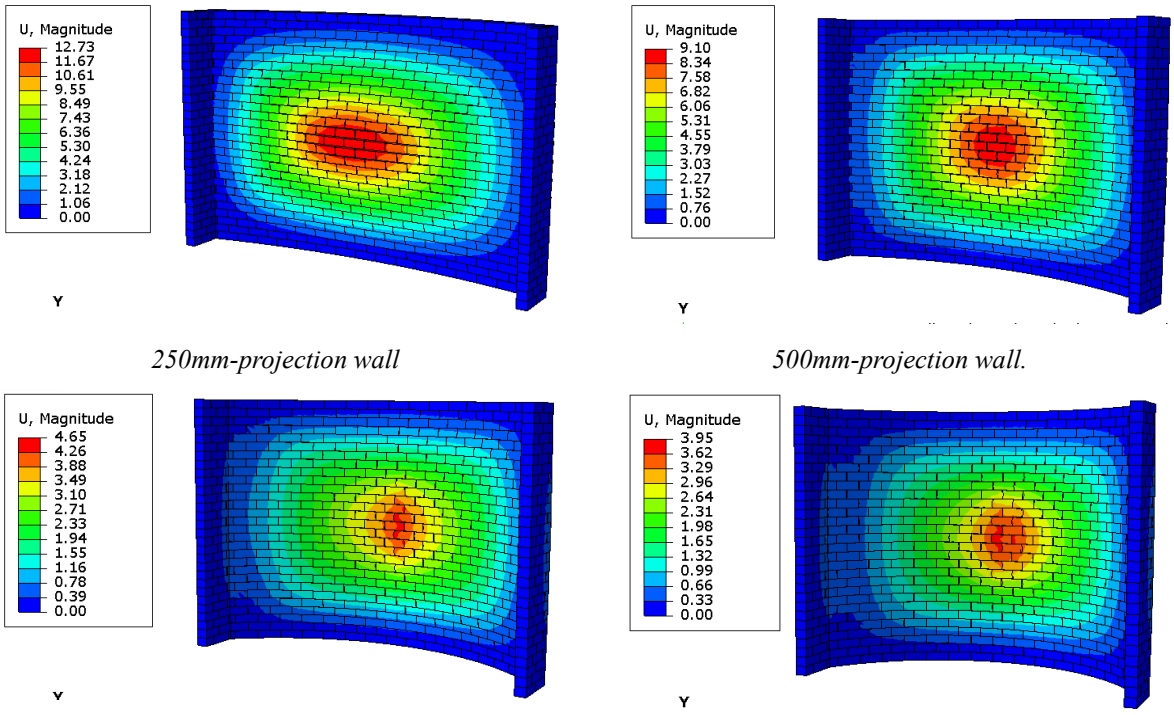

250mm-projection wall *500mm-projection wall.*

750mm-projection wall *1000mm-projection wall.*

Fig. 10: *Displacement contours for curved walls at yielding point*

5. Conclusion

This study successfully developed and validated a numerical model for URM walls using a quasi-static simulation of a straight wall. The model closely reproduced the observed crack pattern, confirming its capability to capture crack initiation and propagation. Overall, the model demonstrates strong fidelity, supporting its use for extended parametric analyses.

The parametric analysis demonstrates that geometrical curvature markedly improves the out-of-plane flexural response of URM walls. Yield pressure increases progressively with projection radius, from 3.0kPa for a straight wall to 7.4kPa for a 1000 mm-projection wall, representing a 150% increase. Correspondingly, yield displacements decrease from 9mm to 2.2mm, reflecting enhanced initial stiffness. The improved performance arises from geometric stiffening and the development of in-plane compressive membrane stresses, which delay crack propagation and increase load-bearing capacity. Post-yield behavior indicates higher ductility and energy absorption, with curved walls sustaining stable pressures over larger deformations compared to straight walls. Crack patterns remain predominantly diagonal but become increasingly localized at the wall center with larger projections, indicating efficient stress redistribution and confinement of high-strain regions. The combination of higher yield thresholds, reduced displacements, and improved post-yield stability confirms that curvature effectively enhances structural efficiency, stiffness, and toughness of URM walls under lateral loading. These results provide a quantifiable framework for predicting the OOP behavior of curved masonry walls and inform the design of more resilient masonry structures.

Future studies should broaden laboratory testing of curved masonry walls under varied loads and geometries to refine predictive models. Investigations into alternative bond patterns and cyclic or dynamic actions, such as seismic and wind effects, are needed to evaluate structural resilience. Expanding the use of locally sourced bricks and mortars will strengthen region-specific material models. Further study of curvature effects on stress distribution, lever arm depth, and section modulus is essential to elucidate the mechanisms governing flexural performance and efficiency in unreinforced masonry walls.

References

Abdulla, H. R., Lourenço, P. B., & Sluys, L. J. (2017). Simplified micro-modelling of unreinforced masonry walls subject to out-of-plane loading. *The Journal of The Masonry Society*, *36*(1), 1–17.

Abdulla, K. (2019). *Numerical investigation into the out-of-plane response of unreinforced masonry walls*. (Doctoral dissertation). The University of Newcastle.

Abdulla, K., Ma, G., & Gad, E. (2017). Investigation into the out-of-plane response of unreinforced masonry walls using simplified macro-model approach. *Structures*, *11*, 268-283.

Alam, M. S., Maalej, M., & Al-Amri, K. (2009). A generalized micromechanical constitutive model for the behaviour of concrete structures. *International Journal of Structural Engineering*, *1*(2), 173–193.

Altunişik, A. C., Kılıç, M., Şahan, M. F., & Genç, F. (2018). Numerical and experimental analysis of curved unreinforced masonry walls. *International Journal of Structural Integrity*, *9*(3), 362–378.

Asteris, P. G., Tasiopoulou, P., & Plevris, V. (2014). Non-linear analysis of masonry shear walls with a finite element modeling approach. *Frontiers in Built Environment*, *1*(4).

Avasthi, R., & Rai, D. C. (2022). Numerical modeling and experimental validation of small-scale masonry arches. *Proceedings of the 12th National Conference in Earthquake Engineering, Earthquake Engineering Research Institute*. (Cited as 2021 in text, corrected to 2022 proceedings).

Baluch, M. H., Al-Otaibi, A. J., & Al-Sulaimani, S. M. (2012). Numerical modeling of structures, combining physical and numerical models. *Journal of Applied Mathematics*, *2012*, 1–11. https://www.google.com/search?q=https://doi.org/10.1155/2012/653063

Basha, S., & Kaushik, H. B. (2015). Response of masonry wallettes and prisms under monotonic and cyclic compression. *Journal of Structural Engineering*, *141*(2), 04014112.

Benzeggagh, M. L., & Kenane, M. (1996). Measurement of mixed-mode fracture energy of adhesively bonded joints using the modified beam test. *Journal of Adhesion Science and Technology*, *10*(3), 221–237.

Benzeggagh, M. L., & Kenane, M. (1996). Measurement of mixed-mode delamination fracture toughness of unidirectional glass/epoxy composites with mixed-mode bending apparatus. *Composite Science and Technology*, *56*(4), 439-449.

Bolhassani, S. P., Ma, G., & Abdulla, K. (2015). Nonlinear dynamic analysis of masonry structures subjected to seismic loading using the micro-modeling approach. *Computers and Structures*, *159*, 166-177.

Bolhassani, S., Koutromanos, I., & Lourenço, P. B. (2015). Simplified anisotropic constitutive model for masonry. *Engineering Structures*, *104*, 148–158. https://doi.org/10.1016/j.engstruct.2015.09.020

Brick Industry Association. (2005). *Technical Note: Curved Walls*. BIA.

Briseghella, B., Frangedaki, E., Gao, X., Lagaros, N. D., & Marano, G. C. (2019). Fujian Tulou Rammed Earth Structures: Optimizing Restoration Techniques Through Participatory Design and Collective Practices. *Procedia Manufacturing*, *44*, 92–99.

British Standards Institution (BSI). (1992). BS 5628-1: Code of practice for use of masonry. Part 1: Structural use of unreinforced masonry. BSI.

Caddemi, S., D'Amico, F., & Fiasconaro, G. (2017). Nonlinear Modelling of Curved Masonry Structures after Seismic Retrofit through FRP Reinforcing. *Applied Sciences*, *7*(3), 79. https://www.google.com/search?q=https://doi.org/10.3390/app7030079

Calladine, C. R. (2007). *Plasticity for engineers*. CRC Press.

Campilho, R. D. S. G., de Moura, M. F. S. F., & Domingues, J. J. M. (2008). Numerical analysis of the quadratic stress criterion for mixed-mode cohesive zone models. *The Journal of Adhesion*, *84*(9), 743–761.

Chang, D., Li, B., & He, B. (2021). Experimental and numerical study on the out-of-plane behaviour of curved unreinforced masonry walls. *Construction and Building Materials*, *281*, 122557.

Chang, Z., Chen, Z., & Chen, J. (2021). New constitutive model for interface elements in finite-element modeling of masonry structures under in-plane shear. *Structures*, *31*, 658–671. https://www.google.com/search?q=https://doi.org/10.1016/j.istruc.2021.02.043

Drucker, D. C., & Prager, W. (1952). Soil mechanics and plastic analysis or limit design. *Quarterly of Applied Mathematics*, *10*(2), 157-165.

European Committee for Standardization (CEN). (2006). EN 1996-3: Eurocode 6: Design of masonry structures – Part 3: Simplified calculation methods for unreinforced masonry structures. CEN.

Fam, A., El-Haddad, T., & Gendy, E. (2015). Out-of-plane behavior of unreinforced masonry walls strengthened with near-surface mounted glass fiber-reinforced polymer bars. *Journal of Composites for Construction*, *19*(3), 04014059.

Galati, N., Tumialan, G., & Nanni, A. (2005). Strengthening with FRP bars of URM walls subject to out-of-plane loads. *ACI Structural Journal*, *102*(4), 512–519.

Godio, M., & Beyer, K. (2019). Out-of-plane stability of unreinforced masonry walls under wind loading. *Journal of Structural Engineering*, *145*(10), 04019102.

Huang, K. P., Li, X., Wu, T., Lin, F., & Guo, J. (2024). Influence of phase change materials on the thermal performance of hollow bricks under cold climate conditions. *E3S Web of Conferences*, *542*, 01009. https://www.google.com/search?q=https://doi.org/10.1051/e3sconf/202454201009

Iqbal, M. J., Gul, A., Badrashi, Y. I., Shah, S. A. A., Badshah, E., Hassan, Z., & Ahmed, W. (2021). Constitutive material model for block masonry and its mechanical properties. *Journal of Mechanics of Continua and Mathematical Sciences*, *16*(4), 61–74. https://www.google.com/search?q=https://doi.org/10.26782/jmcms.2021.04.00005

Jiang, J., Chen, Z., & Chen, J. (2010). Simplified micro-modelling of unreinforced masonry shear walls for dynamic analysis. *Construction and Building Materials*, *24*(12), 2419–2433. https://doi.org/10.1016/j.conbuildmat.2010.05.006

Jinwuth, W., Samali, B., & Wang, C. (2011). Pushover testing of circular adobe structure. In *Advanced Materials Research* (Vol. 287-290, pp. 1907–1910). Trans Tech Publications.

Kaushik, H. B., Morandi, P., Magenes, G., & Rossetto, T. (2007). Stress-strain characteristics of clay brick masonry under uniaxial compression. *Journal of Materials in Civil Engineering*, *19*(10), 882-894.

Khaleel, Z., Ma, G., & Abdulla, K. (2021). Effect of geometrical parameters on the out-of-plane response of semi-circular unreinforced masonry walls. *Engineering Structures*, *244*, 112776.

Khattak, A. S., Mahmood, S., & Khan, M. I. (2021). Experimental and numerical study of confined and unconfined masonry assemblages under compression. *Construction and Building Materials*, *273*, 121703.

Lourenço, P. B., Rots, J. G., & Houtman, M. A. A. (2006). Two approaches for the analysis of masonry structures: Micro and macro-modelling. *Advanced Computational Methods in Engineering*, 223–232.

Maccarini, A., Boscato, G., & Frassine, G. (2018). Flexural Strengthening of Stone Masonry Walls Using Textile-Reinforced Sarooj Mortar. *Applied Sciences*, *8*(12), 2419. https://doi.org/10.3390/app8122419

MacGregor, J. G., & Wight, J. K. (2018). *Reinforced concrete: Mechanics and design* (7th ed.). Pearson.

Maria, G., Ma, G., & Abdulla, K. (2018). Numerical analysis of out-of-plane behavior of unreinforced masonry walls with openings. *Structures*, *16*, 290-305.

Mathew, S., Al-Otaibi, K. O., & Al-Kharraz, A. (2021). Out-of-plane seismic behavior of URM walls strengthened with cementitious-based composite. *Construction and Building Materials*, *300*, 124036.

Misir, I. S., & Yucel, T. (2023). A micro-modeling approach for the seismic assessment of masonry buildings under biaxial loading. *Computers and Structures*, *278*, 106981.

Morandi, P., D'Ayala, D., & Da Porto, F. (2008). In-plane and out-of-plane behavior of curved masonry structures. *Journal of Earthquake Engineering*, *12*(sup1), 162-178.

Noor-E-Khuda, S., & Mahmood, S. (2016). Assessment of in-plane and out-of-plane seismic demands on masonry walls. *Engineering Structures*, *125*, 223–239. https://doi.org/10.1016/j.engstruct.2016.07.009

Osorio, E., Morandi, P., & Magenes, G. (2024). Numerical analysis of the out-of-plane response of curved unreinforced masonry walls. *Engineering Structures*, *302*, 116027.

Plevris, V. G., & Asteris, P. G. (2014). An alternative way of modeling the nonlinear behavior of masonry in-plane walls. *Key Engineering Materials*, *628*, 9-16.

Ram Parajuli, H., & Ghimire, A. (2021). Investigation on Lateral Loading on Masonry Walls. *Nepal Journal of Science and Technology*, *19*(2), 33–40. https://www.google.com/search?q=https://doi.org/10.3126/njst.v20i1.39385

Richter, C., & Brehm, M. (2009). Simplified analysis of unreinforced masonry walls subjected to out-of-plane loading. *The 11th Canadian Conference on Earthquake Engineering*.

Samali, B., Vun, P., & Jinwuth, A. (2011). *Out-of-plane seismic performance of adobe walls reinforced with geogrid mesh*. Paper presented at the 9th Pacific Conference on Earthquake Engineering, Auckland, New Zealand.

Simulia. (2014). *Abaqus analysis user's guide*. Dassault Systèmes.

Tariq, M., Al-Khayyat, A., & Papanikolaou, V. K. (2023). Simplified analytical model for out-of-plane capacity of circular unreinforced masonry walls. *Engineering Structures*, *276*, 115372. https://www.google.com/search?q=https://doi.org/10.1016/j.engstruct.2022.115372

Teschemacher, F., Scheideler, T., & Graf, W. (2023b). Parametric CAD-integrated simulation of masonry structures with geometric and material non-linearity. *Structural Engineering and Mechanics*, *85*(2), 221–234.

Teschemacher, F., Scheld, C., & Lemos, J. V. (2023). Validation of a micro-modelling approach for masonry under out-of-plane loading using the Discrete Element Method. *Engineering Structures*, *290*, 116410.

Urugal, M. (2018). Parametric study on the in-plane behavior of semi-circular masonry arches. *Journal of Structural Engineering*, *144*(11), 04018214.

Vaculik, J., & Griffith, M. (2017). Out-of-plane capacity of slender masonry C-shaped walls. *Engineering Structures*, *147*, 1-13.

Walsh, K. Q., Moon, A. G., & Ingham, J. M. (2017). Out-of-plane seismic performance of retrofitted URM cavity walls from the 2010/2011 Canterbury earthquakes. *Engineering Structures*, *140*, 453–465. https://doi.org/10.1016/j.engstruct.2017.02.049

Wang, Z., Li, B., & Chen, G. (2018). Global stock of buildings and corresponding environmental impact. *Applied Energy*, *225*, 1032–1040. https://doi.org/10.1016/j.apenergy.2018.05.021

Wani, A., Iqbal, S. S., & Ahsan, M. (2023). Numerical simulation of masonry infilled reinforced concrete frames using cohesive zone model. *Construction and Building Materials*, *365*, 130099.

Wilding, D. J., & Beyer, K. (2016). Simplified moment–curvature relationships for unreinforced masonry walls subject to out-of-plane loading. *Journal of structural engineering*, *142*(12), 04016142. https://doi.org/10.1061/(ASCE)ST.1943-541X.0001608

Wilding, D. J., & Beyer, K. (2016). Simplified moment–curvature relationships for unreinforced masonry walls subject to out-of-plane loading. *Journal of structural engineering*, *142*(12), 04016142. https://doi.org/10.1061/(ASCE)ST.1943-541X.0001608

Young, W. C., & Budynas, R. G. (2002). *Roark's formulas for stress and strain*. McGraw-Hill.

Zeng, W., & Li, C. (2023). A review of experimental studies on the in-plane seismic behavior of masonry walls strengthened with textile-reinforced mortar (TRM). *Structures*, *52*, 1–13. https://doi.org/10.1016/j.istruc.2023.03.003

Zeng, W., Zhou, Z., & Chen, J. (2021). A micro-mechanical model for masonry with non-linear Drucker-Prager plasticity. *International Journal of Solids and Structures*, *216*, 159-174.